Thermoelectric Performance of Cu1-xAgxInTe2 Diamond-like Materials with Pseudocubic Crystal Structure

Journal:	*Inorganic Chemistry Frontiers*
Manuscript ID	QI-RES-05-2016-000162.R1
Article Type:	Research article
Date Submitted by the Author:	26-Jun-2016
Complete List of Authors:	Liu, Ruiheng; shanghai Institute of ceramics, CAS, Qin, Yuting; Shanghai Institute of Ceramics, Cheng, Nian; Shanghai Institute of Ceramics CAS Zhang, Jiawei; Shanghai Institute of Ceramics Chinese Academy of Sciences Shi, Xun; Shanghai Institut of Ceramics CAS Grin, Yuri; MPI CPfS, Chemical Metals Science chen, lidong; shanghai institute of ceramics, chinese academy of sciences, CAS Key laboratory of Materials for Energy Conversion

SCHOLARONE™
Manuscripts

Thermoelectric Performance of $Cu_{1-x-\delta}Ag_xInTe_2$ Diamond-like Materials with Pseudocubic Crystal Structure

Ruiheng Liu[1], Yuting Qin[1], Nian Cheng[1], Jiawei Zhang[1], Xun Shi[1*], Yuri Grin[2*], Lidong Chen[1,3,*]

[1]*State Key Laboratory of High Performance Ceramics and Superfine Microstructure, Shanghai Institute of Ceramics, Chinese Academy of Sciences, Shanghai 200050, China*

[2]*Max-Planck-Institut für Chemische Physik fester Stoffe, Nöthnitzer Str. 40, 01187 Dresden, Germany*

[3]*Shanghai Institute of Materials Genome, Shanghai 200444, China*

Abstract

Multiple degenerated bands engineering has been established as an effective approach to maximize electrical transport in thermoelectric materials. A series of polycrystalline samples of chalcopyrite $Cu_{1-x-\delta}Ag_xInTe_2$ (x = 0 - 0.5, δ = 0.02 - 0.05) was synthesized, to achieve multiple degenerated bands. The pseudocubic structure is realized when x is around 0.2. As a result, the degenerated valence bands influence the electrical transport significantly. In addition, the lattice thermal conductivity is significantly depressed in the solid solution due to the strong phonon scattering by strain-field fluctuations, since Ag substitution bring significant anharmonicity to the crystal structure. Highest ZT of 1.24 was obtained at the composition $Cu_{0.75}Ag_{0.2}InTe_2$. This study provides an example how the pseudocubic crystal structure is applied to design and evaluate the TE properties in diamond-like compounds.

Keywords: Thermoelectricity; Pseudocubic symmetry; Diamond-like crystal structure; Strain-field fluctuation

1. Introduction

As an alternative energy recycling technology, thermoelectric (TE) material energy conversion directly converting of heat to electricity, can provide sources of clean energy by utilizing industrial waste heat and increase energy conversion efficiency. The TE performance of the materials is characterized by the dimensionless figure of merit, $ZT = S^2\sigma T/\kappa$, where S, σ, κ and T are the Seebeck coefficient, electrical conductivity, thermal conductivity and absolute temperature, respectively. The state-of-art materials with high ZT require a low thermal conductivity as well as the excellent electrical transport characterized by a large power factor $PF=S^2\sigma$.

The optimal electronic properties of a thermoelectric semiconductor depend primarily on the weighted mobility[1,2], $\sim\mu N_v(m^*)^{3/2}$, here m^* is the effective mass, μ is the mobility of charge carriers, and N_v is the valley degeneracy of the bands. Generally, the carrier effective mass and mobility in solids are in conflict with each other[1-3], i.e. large effective mass usually means low mobility and *vice versa*. Thus highly degenerated or multi-valley band structures[2-4] are required to maximize power factors and excellent electrical properties. As a consequence, the state-of-art TE materials are usually limited to several classes of compounds with high-symmetrical crystal structures, such as PbTe[2,3], skutterudites[5], $Si_{1-x}Ge_x$[1,2], and Bi_2Te_3[1,2], half-Heusler phases[6], Mg_2Si[7], and liquid-like Cu_2Se[8], since their cubic or hexagonal crystal structures yield multi-band structures. This severely extends the exploration of TE materials to low-symmetrical semiconductors, such as compounds with diamond-like crystal structures, called hereafter as diamond-like compounds.

As a class of traditional semiconductors, multi-component diamond-like compounds with tunable band gaps have drawn considerable attention in the photovoltaic application and optical devices. Their TE properties had been not fully valued for a long time. The main obstacle is to optimize electrical and thermal transports simultaneously in the compounds with distorted crystal structures. Binary sphalerites have high-symmetry cubic structures, but their thermal conductivity is too high. Recently, several compounds with low-symmetrical crystal structures (i.e. Cu_2MSe_3, M = Sn, Ge[9,10]; Cu_3SbQ_4, Q = Se,S [11-13]) have been found to exhibit very

low thermal conductivity, however, severe lattice distortion also depresses electrical performance. In face of this contradiction, I-III-VI_2 chalcopyrites provide a perfect solution. Both of $CuInTe_2$ and $CuGaTe_2$ possess excellent electrical properties as well as a low thermal conductivity[14-16]. The reported high *ZT* values (1.18 for $CuInTe_2$ and 1.4 for $CuGaTe_2$) are among the top diamond-like semiconductors, making I-III-VI_2 chalcopyrites to new class of promising thermoelectric materials. Furthermore, by combing theoretical calculations and experimental data[14-21], a simple "unity-η rule" was proposed to screen and design high performance chalcopyrite TE compounds[21]. The key point of the "unity-η rule" is that when tetragonal distortion parameter η (defined as $\eta = c/2a$, where *a* and *c* are the lattice parameters) approaches unity, two valence bands Γ_{4v} and Γ_{5v} tend to degenerate at the edge, yielding good electronic properties(Figure 1). The "unity-η rule" is simple but builds a straightforward bridge between the TE performance and crystal structure projected into lattice parameters. This provides a direct strategy for guiding the evaluation of TE performance in chalcopyrites. This effective approach have been successfully applied recently also to the Zintl phases of the $CaAl_2Sb_2$ type[22].

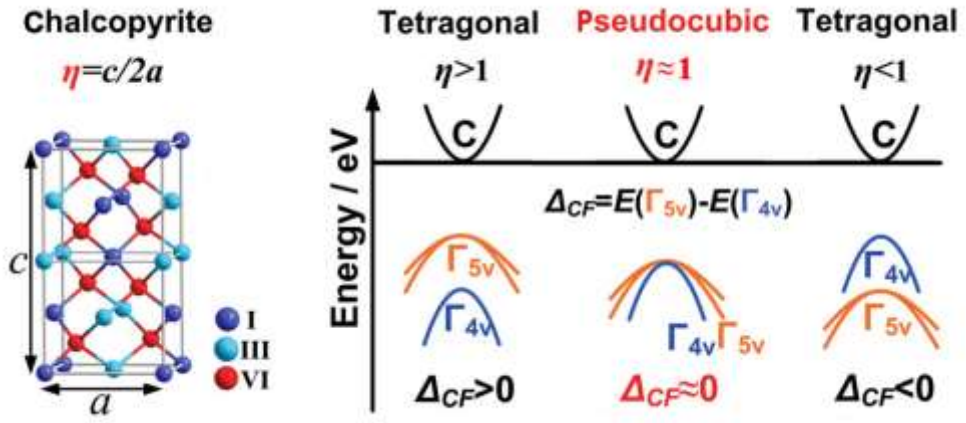

Fig. 1. Crystal structure and electronic bands in ternary chalcopyrites. The pseudocubic structure shows $\eta \approx 1$, and the split bands Γ_{4v} and Γ_{5v} nearly degenerate at the top of valence band.

The "unity-η rule" can also be used to design new pseudocubic multi-component high-performance TE chalcopyrites. Compared with binary sphalerites, the tetragonal distortion of I-III-VI_2 chalcopyrites is weak but still unavoidable. Thus the

degeneration of valence bands near the band edge is unlikely realized in many I-III-VI_2 compounds when η values deviated from unity. Therefore, by mixing two host compounds with opposite distortions in *c/2a* is an expected effective way to achieve band degeneration in a pseudocubic structure, thus, good electrical properties as well as TE performance[21,22]. In addition, the thermal conductivity in I-III-VI_2 chalcopyrites is still rather high compared with the state-of-art thermoelectric materials. The massive point defects caused by formation of disordered solid solutions could in additionally greatly depress the thermal conductivity due to mass and stress-field fluctuations[23, 24]. In this work, we choose $CuInTe_2$ ($\eta \approx 1.004$[21, 25]) and $AgInTe_2$ ($\eta \approx 0.981$[26]) as the two precursors to design and realize pseudocubic crystal structure in a solid solution for good electrical properties and low lattice thermal conductivity. High *ZT* 1.24 for pseudocubic $Cu_{0.75}Ag_{0.2}InTe_2$ is achieved.

2. Experimental details

Bulk polycrystalline samples $Cu_{1-x-\delta}Ag_xInTe_2$ (x = 0.1 - 0.5, δ = 0.0, 0.02 and 0.05) were prepared by sequential melting, grinding, annealing, and sintering. Because fully stoichiometric chalcopyrite compounds are semiconductors, samples with small Cu deficiency were prepared in order to achieve compositions with optimized hole concentration and electrical properties. Elements Cu (Alfa Aesar, 5N, shot), Ag (Alfa Aesar, 5N, granule), In (Alfa Aesar, 5N, granule), and Te (Alfa Aesar, 5N, shot) were loaded into graphite crucibles, and then sealed in evacuated silica tubes. The silica tubes were heated to 1100 ºC and kept at this temperature for 12 hours, then quenched in ice cold-water and annealed at 650 ºC for 5 days. The obtained ingots were crushed into fine powder for sintering. All densified bulk samples $Cu_{1-x-\delta}Ag_xInTe_2$ (x = 0.1 - 0.5) were consolidated by Spark Plasma Sintering (SPS) at about 550 °C for 10 minutes under a uniaxial pressure of 50 MPa in vacuum. In comparison, the samples $Cu_{1-x-\delta}Ag_xInTe_2$ (x = 0.1 - 0.3) were also consolidated by Hot Pressing (HP) for 20 minutes at 650 ºC under a pressure of 65 MPa.

The phases constituting the samples were evaluated by powder X-ray diffraction (XRD), which was carried out on a diffractometer Rigaku 69 D/max2250 (Cu-K radiation, 40 kV/200 mA); Si powder (a = 5.431 Å) was used as internal standard

when running X-ray diffraction measurements. The compositional homogeneity of all the samples was examined by electron probe microanalysis (EPMA, JEOL JXA-8100). Optical absorption spectra by using pulverized powders were measured at room temperature by a UV-visible-near IR spectrometer (HITACHI U-3010) equipped with an integrating sphere. Seebeck coefficient and electrical resistivity were measured in the temperature of 300-750 K using a ZEM-3 system under a sealed chamber with a small amount of helium gas. Thermal diffusivity (D) was measured using the laser flash method (Netzsch, LFA427). The electrical and thermal properties were measured to 850 K for HP samples, and to 750 K for SPS samples like it was made previously for $Cu_2Sn_{1-x}Ga_xSe_3$[27]. The gravimetric density (d) was measured by the Archimedes method. Hall effect measurements were performed for HP samples using a cryostat equipped with a 5.5 T magnet.

3. Results and discussion

3.1 Phase and structure characterization

Since samples with different Cu deficiency at each Ag content show very close crystal structure parameter and performance, we choose samples with best electrical property at each Ag content for the following discussion. The XRD patterns of $Cu_{1-x-\delta}Ag_xInTe_2$ (x = 0.1 - 0.3) were shown in Fig. 2(a). All the XRD peaks are assigned to the diffraction patterns of chalcopyrite structure with the space group $I\bar{4}2d$. No other impurity peaks are found. The EPMA analysis for x = 0.2 sample confirmed that Cu, Ag, In, and Te were uniformly distributed, as shown in Fig. 2(b). The chemical compositions of samples with x = 0.1 - 0.3 detected by the quantitative EDS analysis were listed in Table I.

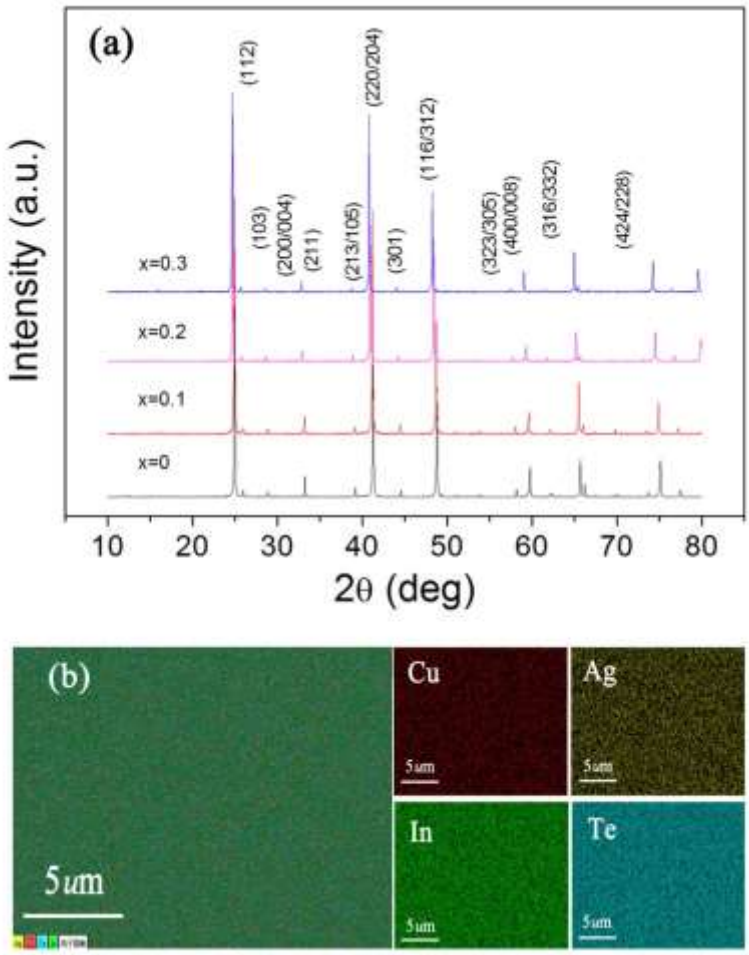

Fig. 2. (a) X-ray powder diffraction patterns of $Cu_{1-x-\delta}Ag_xInTe_2$ solid solution (x = 0.1 - 0.3); (b) EPMA-filtered secondary X-ray element maps of HP- $Cu_{0.75}Ag_{0.2}InTe_2$.

Table I: Chemical composition of $Cu_{1-x-\delta}Ag_xInTe_2$ samples.

Sample	Composition (at.%)			
	Cu	Ag	In	Te
$CuInTe_2$	24.92 ± 0.71	--	25.60 ± 0.36	49.48 ± 0.51
$Cu_{0.88}Ag_{0.1}InTe_2$	21.11 ± 0.42	2.73 ± 0.19	25.95 ± 0.21	50.21 ± 0.30 *
	23.61 ± 0.49	2.70 ± 0.19	24.76 ± 0.27	48.92 ± 0.55**
$Cu_{0.75}Ag_{0.2}InTe_2$	18.29 ± 0.39	4.77 ± 0.16	26.20 ± 0.28	50.74 ± 0.41*
	20.59 ± 0.57	5.49 ± 0.20	25.18 ± 0.42	48.73 ± 0.55**
$Cu_{0.68}Ag_{0.3}InTe_2$	16.49 ± 0.53	7.41 ± 0.21	25.74 ± 0.20	50.36 ± 0.45*
	18.92 ± 0.48	7.36 ± 0.29	24.83 ± 0.32	48.89 ± 0.58**

* sample densified by HP
** sample densified by SPS

Since the atomic radius of Ag (1.44 Å) is larger than Cu (1.28 Å), the XRD peak positions slightly shift to low angles with the Ag content increasing, revealing the lattice expansion by Ag substituting Cu atoms. The lattice parameter refinement of the

samples was performed with the software WinCSD[28]. As shown in Fig. 3, both the lattice parameter *a* and *c* increase almost linearly as the Ag content increasing, being consistent with the Vegard's rule. Linear fitting the experimental data gives the following $a(x)$ and $c(x)$ equations in the solid solution $Cu_{1-x-\delta}Ag_xInTe_2$: $a = 6.1908 + 0.2200x$, and $c = 12.4289 + 0.1961x$. The gradient slope of parameter *c* ($b_2 = 0.1961$) is slightly lower than that of parameter *a* ($b_1 = 0.2200$), indicating that the lattice expansion along *x* axis is more significant than that along *z* axis. Consequently, the distortion parameter $\eta = c/2a$ decreases with increasing Ag content, and equals to unity when $x = 0.19$ according to fitting result. This is consistent with the experimental data that unity of η is almost obtained in the sample $Cu_{0.75}Ag_{0.2}InTe_2$ ($\eta \approx 1.0003$). Previous work Rietveld refinement revealed that the pesudocubic tetragonal unit cell should be achieved at the composition $x = 0.25$[26]. The unity-η of the pseudocubic structure without long range distortion is favorable for realizing highly degenerated valence band and then good TE performance[21](see below).

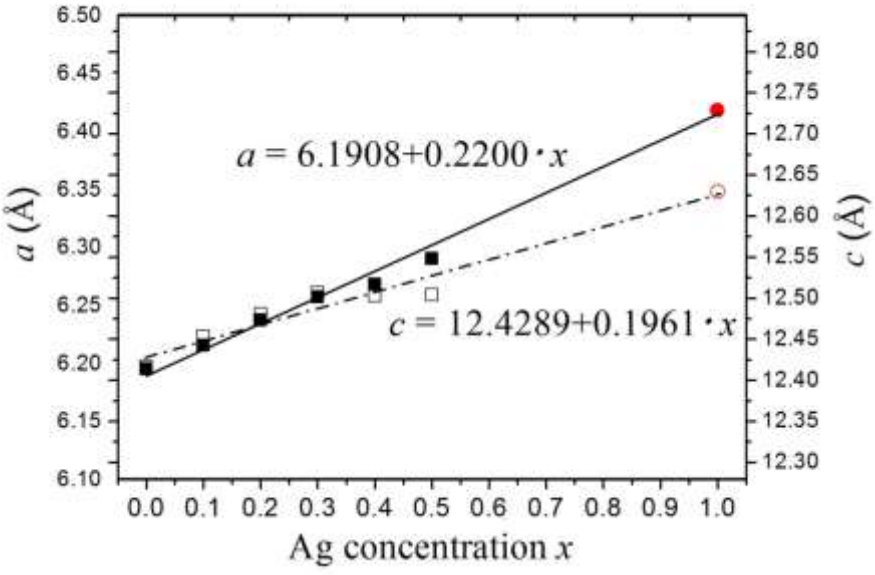

Fig. 3. Variation of lattice parameters *a* and *c* *vs* Ag content in the $Cu_{1-x-\delta}Ag_xInTe_2$ ($x = 0$ - 0.5) solid solution.

Table II: Lattice parameters, and band gap in $Cu_{1-x-\delta}Ag_xInTe_2$ ($x = 0$ - 0.5) sample powders.

Compostion	Lattice parameters			E_g (eV)	Sample Code
	a (Å) (±0.0006)	*c* (Å) (±0.0009)	$\eta = c/2a$		

$CuInTe_2$	6.1958	12.4162	1.002 (1.003[25])	0.95 (1.04[25],1.06[29])	-
$Cu_{0.88}Ag_{0.1}InTe_2$	6.2161	12.4532	1.002	0.96	Ag0.1
$Cu_{0.75}Ag_{0.2}InTe_2$	6.2379	12.4804	1.000	0.93	Ag0.2
$Cu_{0.68}Ag_{0.3}InTe_2$	6.2578	12.4965	0.998	0.90	Ag0.3
$Cu_{0.55}Ag_{0.4}InTe_2$	6.2684	12.5026	0.997	0.89	Ag0.4
$Cu_{0.45}Ag_{0.5}InTe_2$	6.2907	12.5037	0.993	0.89	Ag0.5
$AgInTe_2$	6.4430[26]	12.6357[26]	0.981[26]	0.96[29]	-

3.2 Band structure and Electrical transport

3.2.1 Optical properties and band gap

The absorption coefficients α were estimated from the absorption spectrum of $Cu_{1-x\delta}Ag_xInTe_2$. At room temperature, the optical data plotted as $(\alpha h\upsilon)^2$ against photon energy is shown in Fig. 4, where α is the absorption coefficient, h is the Planck constant, and υ is the wave number. The extrapolation of the linear part of the $(ah\upsilon)^2$ curve gives the estimated E_g for $Cu_{1-x-\delta}Ag_xInTe_2$, from 0.96 eV to 0.89 eV as listed in Table II. The band gap obtained here is slightly lower than the previous reported data. For example, the gap of $CuInTe_2$ for 1.05-1.1eV was reported in Ref. 25, 29. When increasing Ag content, the band gap exhibits a slight decrease, being agreement with the narrow band gap of $AgInTe_2$[29-32]. In the chalcopyrite structure, the strong *p–d* orbital hybridization results in a considerable contribution to the near-edge valence bands[33]. As compared with the *3d* orbitals in Cu, the Ag-4*d* orbitals could slightly elevate the valence band edge and thus to slightly reduce the band gap.

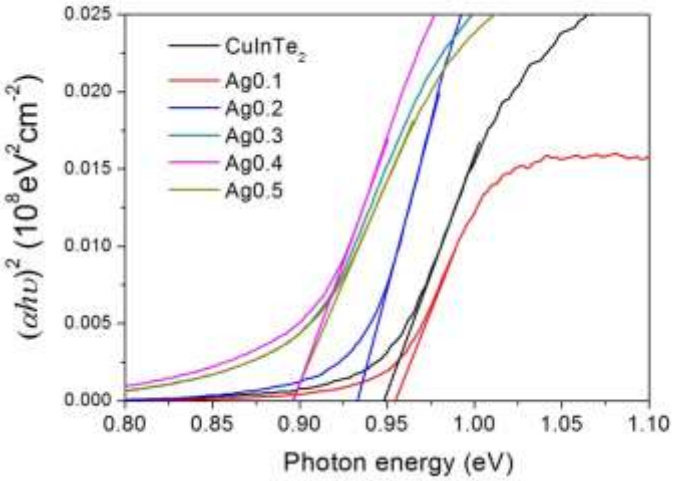

Fig. 4. Photon energy dependence of $(\alpha h\upsilon)^2$ for $Cu_{1-x-\delta}Ag_xInTe_2$ (x = 0 - 0.5) at room temperature. Extrapolation of the linear part of the dependence to $(\alpha h\upsilon)^2 = 0$ yields the estimated band gap E_g.

3.2.2 Electrical conductivity and Seebeck coefficient

Fig. 5 displays the temperature dependence of electrical conductivity σ and Seebeck coefficient S for the SPS and HP samples $Cu_{1-x-\delta}Ag_xInTe_2$. With the Ag content increasing from x = 0 to 0.5, the electrical conductivity firstly increases due to Cu deficiency and then greatly decreases from 13.5×10^3 Sm^{-1} to 1.1×10^3 Sm^{-1} with Ag substitution at room temperature. This dramatic decline is also observed in $(Cu/Ag)GaTe_2$[34] as well as $(Cu/Ag)_2(Ge/Sn)Se_3$[9,35] and can be explained by the carrier concentration variation (shown below). Meanwhile, the Seebeck coefficient of $Cu_{1-x-\delta}Ag_xInTe_2$ is enhanced drastically with Ag substitution. For example, the room temperature Seebeck coefficient increases from 201 μVK^{-1} in $Cu_{0.88}Ag_{0.1}InTe_2$ to 393 $\mu V/K$ in $Cu_{0.45}Ag_{0.5}InTe_2$. As a result, the power factor PF is initially increased and then gradually decreased when increasing Ag doping content. The highest value of PF is 6 $\mu Wcm^{-1}K^{-2}$ at 300 K in the sample with Ag content of 0.1, as shown in Fig. 6. The room-temperature TE properties are summarized in Table III.

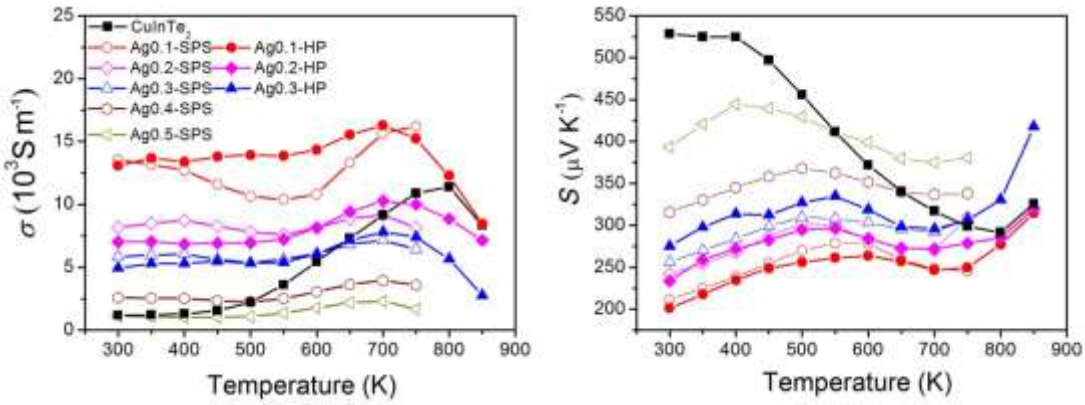

Fig. 5. Temperature dependence of electric transport properties of polycrystalline $Cu_{1-x-\delta}Ag_xInTe_2$ (x = 0 - 0.5); (a) electrical resistivity σ and (b) Seebeck coefficient S.

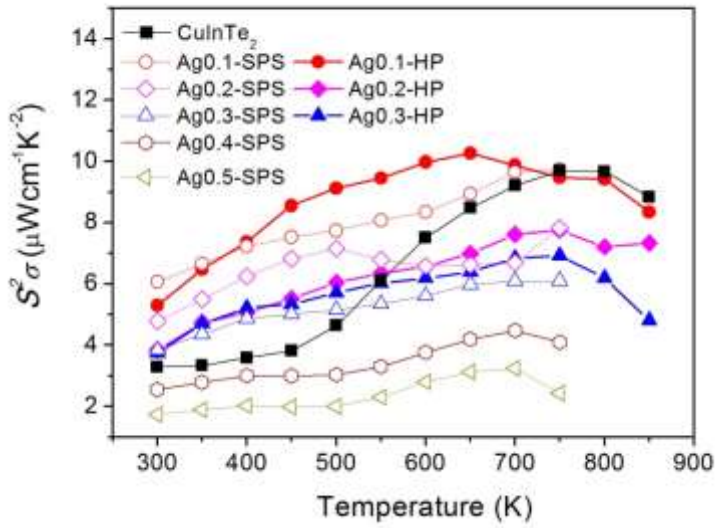

Fig. 6. Power factor as a function of temperature for $Cu_{1-x-\delta}Ag_xInTe_2$ (x = 0 - 0.5).

Table III: TE properties, hole concentration *(p)*, mobility (μ), effective mass (m^*), Lorentz number (L), and phonon scattering parameters (u, Γ_M, Γ_S, *and* ε) of $Cu_{1-x-\delta}Ag_xInTe_2$ (x = 0 - 0.5) samples.

Densification Technique.	Composition	S (μVK^{-1})	σ ($10^3 Sm^{-1}$)	κ ($Wm^{-1}K^{-1}$)	p ($10^{19}/cm^3$)	μ ($cm^2V^{-1}s^{-1}$)	m^*	L ($10^{-8}V^2K^{-2}$)	u	Γ_M	Γ_S	ε
	$CuInTe_2$	528	0.12	6.12	0.07	109	0.90	1.49	-	-	-	-
	$Cu_{0.88}Ag_{0.1}InTe_2$	201	13.5	2.84	1.70	50	1.01	1.61	2.34	0.0037	0.0403	228
HP	$Cu_{0.75}Ag_{0.2}InTe_2$	231	7.1	1.84	1.11	40	0.95	1.58	3.76	0.0064	0.1160	331
	$Cu_{0.68}Ag_{0.3}InTe_2$	275	4.9	1.88	0.75	41	0.99	1.54	3.30	0.0083	0.0939	185
	$Cu_{0.88}Ag_{0.1}InTe_2$	211	14.2	2.90	2.00	44	1.11	1.61	2.27	0.0037	0.0377	213
	$Cu_{0.75}Ag_{0.2}InTe_2$	242	8.2	1.95	1.52	36	1.20	1.57	3.50	0.0064	0.0994	284
SPS	$Cu_{0.68}Ag_{0.3}InTe_2$	256	5.8	1.75	1.18	31	1.14	1.56	3.61	0.0083	0.1142	225
	$Cu_{0.55}Ag_{0.4}InTe_2$	315	2.6	1.54	-	-	-	-	3.78	0.0093	0.1377	216
	$Cu_{0.45}Ag_{0.5}InTe_2$	393	1.1	1.40	-	-	-	-	3.75	0.0095	0.1511	209

3.2.3 Electrical transport and unity-η rule

According to Hall effect measurements, all samples exhibit *p*-type transport and the calculated hole concentrations in the range of 2 K to 300 K are plotted in Fig. 7(a). With similar Cu deficiency, the hole concentration decreases remarkably with the Ag content increasing, which is consistent with the variety of electrical conductivity and Seebeck coefficient. This may be related to the different character of Cu-X and Ag-X chemical bonds influencing the real band structure. Another possibility is that because the Cu-deficient starting composition of the samples, introducing of silver results in both – substitution of copper and filling-up the eventual structural defects. A more deep study is required for the full understanding of this issue is necessary in the future. The value of room temperature hole concentrations are 1.70×10^{19} cm^{-3}, 1.11×10^{19} cm^{-3} and 0.75×10^{19} cm^{-3} for the samples with Ag content of 0.1, 0.2 and 0.3, respectively. The carrier concentrations of all samples are almost constant from 2 K to 300 K, indicating the domination of extrinsic carriers. The hole mobility (μ_H) of $Cu_{1-x-\delta}Ag_xInTe_2$ is also strongly influenced by the substituted Ag atoms at Cu sites. The random distribution of Ag at Cu sites generates additional scattering centers[2]. No matter with the sintering technique, the hole mobility consistently decreases with Ag content increasing. For example, room temperature μ_H is decreased from 125 $cm^2V^{-1}s^{-1}$ in $CuInTe_2$ to 41 $cm^2V^{-1}s^{-1}$ in $Cu_{0.65}Ag_{0.3}InTe_2$ sintered by HP and 31 $cm^2V^{-1}s^{-1}$ in $Cu_{0.65}Ag_{0.3}InTe_2$ sintered by SPS. Except $CuInTe_2$, the carrier mobility of all samples deviates strongly from the $T^{3/2}$ dependence around room temperature. In the samples with high Ag content, the temperature dependence of mobility even approaches $T^{3/2}$ dependence, indicating a ionized impurity scattering[36]. Therefore, in the temperature range below 300 K, the hole mobility is determined by a mixed scattering mechanism, such as acoustic phonon, atomic substitution.

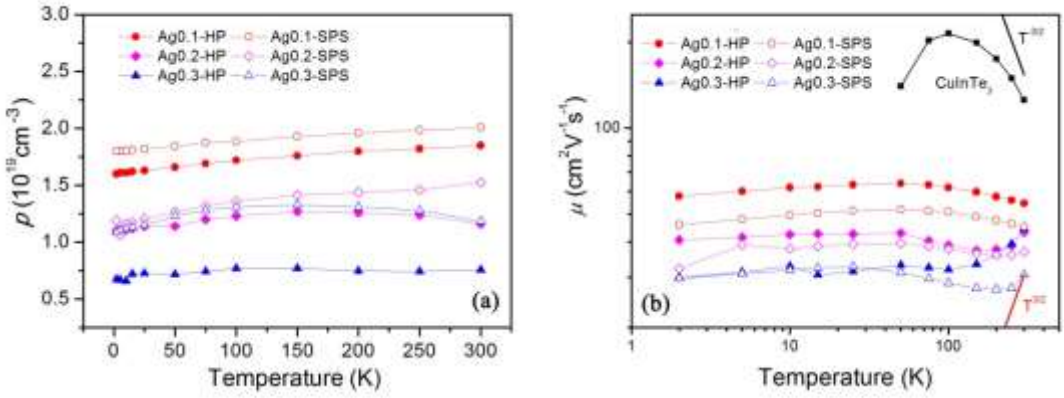

Fig. 7. Temperature dependence of hole concentration $p(T)$ (a) and hole mobility logμ (logT) (b) for $Cu_{1-x-\delta}Ag_xInTe_2$ (x = 0.1 - 0.3) samples.

The mixed scattering mechanism can be also supported by the hole concentration dependence of mobility. As shown in Fig. 8(a), the mobility shows a nearly nice $p^{-1/3}$ relationship (see the solid line) for the materials with dominant acoustic phonon scattering such as $CuInTe_2$ and $CuIn_{1-x}Cd_xTe_2$. However, the mobilities of solution system are far below the line dominated by acoustic phonon scattering due to additional carrier scatterings.

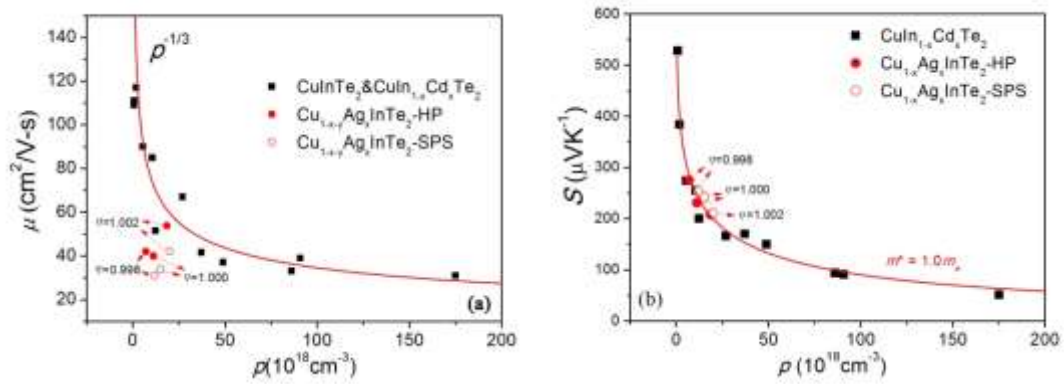

Fig. 8. hole concentration p dependence of the hole mobility μ (a) and Seebeck coefficient S (b) for $Cu_{1-x-\delta}Ag_xInTe_2$ (x = 0 - 0.3) at 300 K. The squares represent experimental data from literature (Refs.14, 18, and 37), and the circles represent our data. The line in (a) gives the $p^{-1/3}$ relationship, the red lines in (b) were generated using the single parabolic band model by taking $m^* = 1.0m_e$ respectively.

Besides the decreased hole concentrations and mobilities, Ag substitution also changes the valence band character caused by the structure evolution. Because chalcopyrite compounds $CuInTe_2$ and $AgInTe_2$ possess non-cubic tetragonal

structures with distorted tetrahedra, in contrast to the zinc blende lattice, the triply degenerated valence band Γ_{15v} in tetragonal chalcopyrites splits into a non-degenerate band Γ_{4v} and a doubly degenerated band Γ_{5v} due to the crystal field effect[38, 39] with the splitting energy defined as $\Delta_{CF} = E(\Gamma_{5v}) - E(\Gamma_{4v})$. The splitting energy Δ_{CF} is approximately described by $\Delta_{CF} = 3b(1-\eta)$, where b is a parameter related with the structure distortion[21,40]. As a result, the Γ_{5v} lies below the Γ_{4v} in $AgInTe_2$ because $\eta < 1$ (Δ_{CF} = -0.09 eV, Ref. 21), while Γ_{5v} lies above Γ_{4v} in $CuInTe_2$ because $\eta > 1$ (Δ_{CF} = 0.01 eV, Ref. 21). Thus, when Ag content is around $x \sim 0.2$, the Γ_{4v} and Γ_{5v} bands tend to degenerate near the valence band edge, thus gradually enhancing power factors ($S^2\sigma$)[41]. As is supported by the data showed in Table III, in which the room-temperature Seebeck coefficient of SPS-$Cu_{0.68}Ag_{0.3}InTe_2$ (256 μVK^{-1}) is higher than that of HP-$Cu_{0.75}Ag_{0.2}InTe_2$ (231 $\mu V/K$) although both of them possess identical hole concentrations.

In the single-parabolic band model, Seebeck coefficient and hole concentration can be linked by the equations[2]:

$$S = \frac{k_B}{q}\left(\xi - \frac{(2+\lambda)F_{\lambda+1}(\xi)}{(1+\lambda)F_{\lambda}(\xi)}\right) \quad (1)$$

and

$$p = 4\pi\left(\frac{m^* k_B T}{h}\right)^{3/2} F_{1/2}(\xi) \quad (2)$$

where ξ, λ, k_B, h and $F_j(\xi)$ are the reduced Fermi energy, the scattering factor, Boltzmann constant, Planck constant and Fermi integral, respectively. Using the measured Seebeck coefficients and hole concentrations, the room temperature effective masses m^* are calculated and listed in Table III. The values of m^* for $Cu_{1-x-\delta}Ag_xInTe_2$ are around 0.95~1.2 m_e, which is higher than the previously reported value for $CuInTe_2$, 0.6~0.8 m_e[14,16]. The red line in Fig. 8(b) represents the calculated results by using the single-parabolic band model with the scattering factor λ is set to be 0 according to the mobility data and $m^* = 1.0\ m_e$. The data of $Cu_{1-x-\delta}Ag_xInTe_2$ and $CuIn_{1-x}Cd_xTe_2$ fits the calculated line quite well in the whole range. For $Cu_{1-x-\delta}Ag_xInTe_2$ materials shown here, x changes from 0 to 0.5, thus parameter η varies in a small

range from 0.992 to 1.002. And the Δ_{CF} changes from -0.09 eV to 0.01 eV as well. Such a small change leads to a small deviation in the effective mass, which is consistent the same trend observed in Fig. 8b. In order to simply the model calculation, we thus use a constant effective mass for Eq. 1 and Eq. 2.

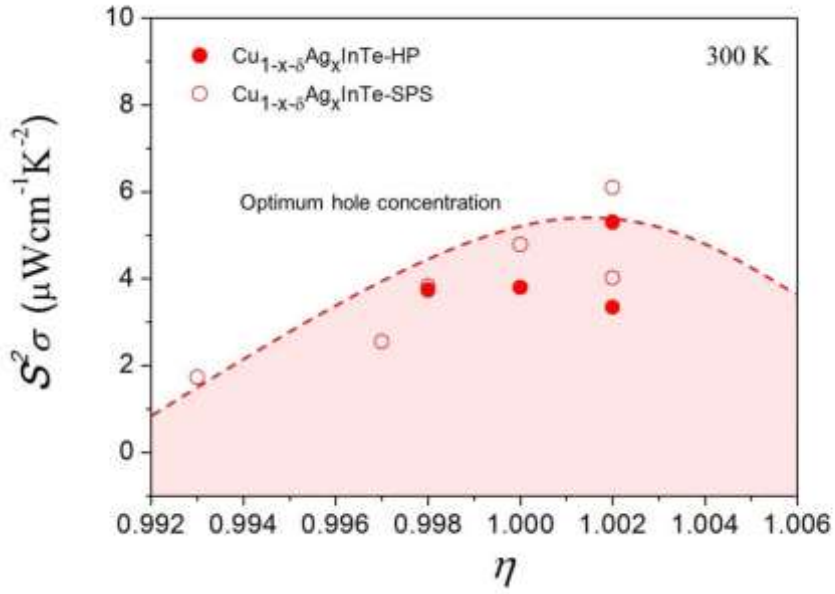

Fig. 9. Power factors as a function of distortion parameter η for $Cu_{1-x-\delta}Ag_xInTe_2$ (x = 0 - 0.5) materials at 300 K. The dashed line is a guide to the eyes, which represents the materials with optimum hole concentrations at various η values.

Furthermore, for optimal power factors in TE compounds, it is desirable that multibands are nearly degenerated at the band edge[3, 7, 21]. The Γ_{5v} and Γ_{4v} bands will completely degenerate at the composition around x = 0.19 in this system based on the theoretical calculations[21, 26] and present study. Fig. 9 shows η dependences of power factors for $Cu_{1-x-\delta}Ag_xInTe_2$. Previous studies revealed that the optimum hole concentrations in $CuInTe_2$-based materials are in the range of 1.0 ~ 3.0 × 10^{19} cm^{-3} [37]. The hole concentrations of all present $Cu_{1-x-\delta}Ag_xInTe_2$ samples are almost among this range, indicating that these materials should have good power factors. In addition, parameter η is another factor to determine power factors. For a given η, the hole concentrations may vary from a very small value (in an intrinsic semiconductor) to a very large value (in a metal). Power factor is small when carrier concentrations are

small or large, but it has a maximum value when carrier concentration is in the optimum range. In Fig. 9, the dashed line represents the materials with optimum carrier concentrations while the area below this line represents for the materials with high or low carrier concentrations. It requires lots of samples with various carrier concentrations and parameter η values to accurately know this best line in Fig. 9, which beyond the current study. We just use a trend line instead of the accurate curve based on our data. Since the samples in this work are mostly within optimum hole concentration range, the variation of power factor is mainly caused by parameter η.

The sintering process also affects the hole transportation as well. Under the same nominal composition $Cu_{1-x-\delta}Ag_xInTe_2$, the HP samples show identical electrical conductivity comparing with SPS samples. In contrast, the hole concentrations in HP samples is lower than those in the SPS samples. Comparing with hot-press sintering, in which the sample is heated by thermal conduction, SPS employs a very large current going through the sample to heat it directly and quickly. Thus the pulsed electric current during the SPS process can cause overheating in local contact surface of particles, leading to melting and/or evaporation of low melting point elements[8,42-44]. In current study, the elements distribution errors were calculated according to data of 20 EDS points performed both on SPS and HP samples. Evidently, the composition fluctuation of SPS samples is larger than that of HP samples, as shown in Table I. The composition inhomogeneity and lattice defects can provide additional scattering to holes and thus greatly affect the electrical properties. As shown in Fig. 7(b) and Fig. 8(a), the hole mobility of SPS samples is lower than the HP samples although their nominal compositions are the same, leading to a reduced electrical conductivity. We also see the deviation for Seebeck coefficients in the SPS and HP samples. But it seems that the impact of sintering process on Seebeck coefficient seems not as notable as on electrical conductivity (see Fig. 5b).

3.3 Thermal conductivity

The thermal conductivity κ was calculated from the specific heat C_P, density d, and thermal diffusivity D, $\kappa = C_P \times d \times D$. Here the specific heat was taken as the Dulong-Petit value ($C = 3k$ per atom). κ can be expressed by the sum of a lattice

component κ_L and a carrier component κ_C as $\kappa = \kappa_L + \kappa_C$. The carrier contribution is calculated according to the Wiedemann-Franz law ($\kappa_C = L\sigma T$), where L is the Lorentz number. Because the electrical conductivities in all samples are as low as in the level of 10^3 Sm^{-1}, the heat carried by holes contributes little to the total thermal conductivity, and the calculated κ_L is very close to κ. The total thermal conductivities of all $Cu_{1-x-\delta}Ag_xInTe_2$ samples are dramatically decreased when increasing temperature and reach around 0.4 $Wm^{-1}K^{-1}$ above 850 K, which are a fairly low level for thermoelectric materials, as shown in Fig. 10. For comparing, the minimum lattice thermal conductivity is calculated from the formula $\kappa = 1/3(v \times l_{min} \times C_V)$, where C_V is the heat capacity per unit volume of the system, v is the sound velocity, and l_{min} is the minimum phonon mean free path, which is generally comparable to materials' nearest interatomic distance[45]. In $Cu_{1-x-\delta}Ag_xInTe_2$, l_{min} is assumed to be 0.260 nm and the velocity of sound v can be roughly considered as the value of $CuInTe_2$ (2002 ms^{-1} from Ref. 45). Based on these assumptions, the κ_{min} should be around 0.3 W/mK, which is almost achieved in $Cu_{0.75}Ag_{0.2}InTe_2$ at 886 K, as displayed in the inset of Fig. 10. The dramatic decrease of κ can be mainly attributed to the Umklapp scattering, as shown by the approximate *1/T* temperature dependence which is also observed in other I-III-VI_2 chalcopyrite compounds[18, 27, 34, 46, 47] and other diamond-like semiconductors[9, 17, 48]. Meanwhile, there is no significant difference between the HP samples and SPS samples with same chemical compositions, revealing that phonon scattering is not sensitive to sintering technique.

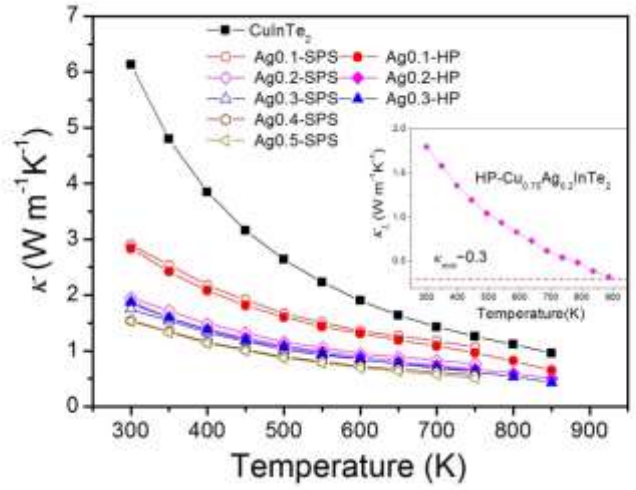

Fig. 10. Temperature dependence of thermal conductivity for $Cu_{1-x-\delta}Ag_xInTe_2$ (x = 0 - 0.5). The inset picture displays lattice thermal conductivity κ_L of HP-$Cu_{0.75}Ag_{0.2}InTe_2$. At 886 K, the value of κ_L hits the κ_{min}.

The Ag substitution in $Cu_{1-x-\delta}Ag_xInTe_2$ solid solution significantly depresses the lattice thermal conductivity. One reason for this depression is considered to be caused by the mass and radius differences between two substituted atoms. In a solid-solution system, the effect of point defects on lattice thermal conductivity can be given by the Callaway–Klemens' equation[23]:

$$\frac{\kappa_L}{\kappa_L^P} = \frac{\tan^{-1}(u)}{u}, \quad u^2 = \frac{\pi^2 \theta_D \Omega}{h v^2} \kappa_L^P \Gamma_{total} \qquad (3)$$

where κ_L^P, u, θ_D, Ω, h, v, and Γ_{total} are the lattice thermal conductivity of pure material without any defects, disorder scaling parameter, Debye temperature, the average volume/atom, the Planck constant, the average lattice sound velocity, and the disorder scattering parameter, respectively. Γ_{total} originates from mass and strain field fluctuations by the point defects[22, 49-51], which are represented by the scattering parameters Γ_M and Γ_S, respectively. Generally, in some system such as skutteruidtes[50, 52-54] or PbTe[3, 55, 56], because the lattice parameters change very little, the effect of strain field fluctuation could be ignored. Hence Γ_{total} is approximately equal to Γ_M. Γ_M can be given by the following equation for the present solid solution:

$$\Gamma_M = \frac{1}{4}\left(\frac{\Delta M_{Cu,Ag}}{\overline{M_m}}\right)^2 \cdot x(1-x) \qquad (4)$$

where $\overline{M_m}$ means the average mass of all the atom in an unit cell. By using the lattice parameters of the samples, the Ω is 2.978×10^{-29} m^3/atom, and the value of Debye temperature and the average lattice sound velocity of $Cu_{1-x-\delta}Ag_xInTe_2$ can be approximately taken the values in $CuInTe_2$[57], which gives θ_D = 197.5K and v = 2002 ms^{-1}. According to Eq.(4) and (5), the calculated κ_L (black dashed line in Fig. 11) is much higher than the experimental results. This indicates that, in chalcopyrites, besides the mass fluctuation effect, the strain-field fluctuations bring by Ag substitution also may play an important role, since Ag expands the lattice significantly.

The strength of strain-field fluctuation effects depends on the size differences and the bonding nature of specific atoms[23, 49, 58], and is given by:

$$\Gamma_S = \frac{1}{4}\left(\frac{\overline{M_{Cu,Ag}}}{\overline{M_m}}\right)^2 \cdot x(1-x)\cdot\varepsilon\cdot\left(\frac{\Delta r_{Cu,Ag}}{\bar{r}}\right)^2 \qquad (5)$$

where r is the radii of atoms, and the parameter ε is a function of the Grüneisen parameter γ, which characterizes the anharmonicity of the lattice. Considering both mass and strain field fluctuations, i.e. $\Gamma_{total} = \Gamma_M + \Gamma_S$, we re-estimate the κ_L at 300 K and 600 K with the parameter ε of 280.The calculated lines (red solid line for 300 K and red dashed line for 600 K) fit perfectly well with the experimental data, as plotted in the Fig. 11. This confirms the important role of strain field fluctuation on phonon scattering in $Cu_{1-x-\delta}Ag_xInTe_2$ solid solutions.

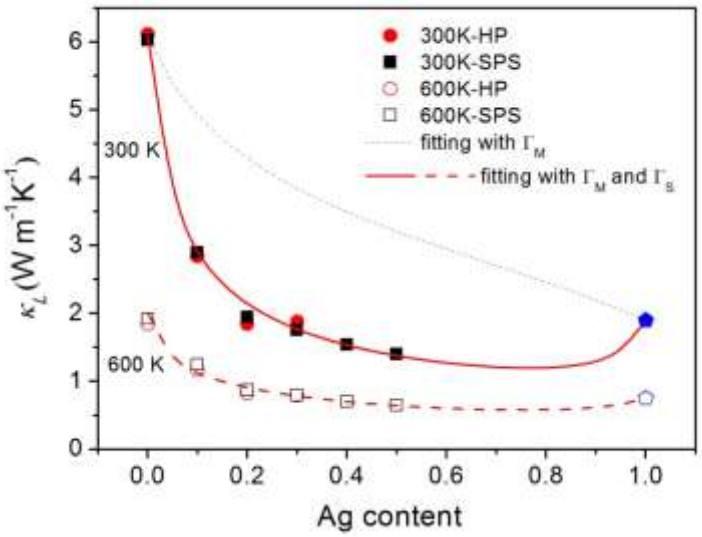

Fig. 11. Lattice thermal conductivity as a function of Ag content in $Cu_{1-x-\delta}Ag_xInTe_2$ (x = 0 - 0.5) at 300 K and 600 K[19]. The black dashed line shows the calculated κ_L only based on the mass fluctuation between Cu and Ag at 300 K, and the red lines represent the calculated κ_L including both mass and strain field fluctuations with $\varepsilon = 280$ at 300 K and 600 K.

To distinguish the respective contribution from the mass and strain field fluctuations, we estimates the Γ_M, Γ_S and ε for each sample by using the experimental κ_L based on Eq. (3)-(5), which are listed in Table III. The Γ_M for all samples are in the range of 0.003 ~ 0.009, while the Γ_S are much higher than Γ_M by a degree of one or two orders. Γ_S varies considerably from 0.04 to 0.15 and it roughly increases with the Ag content increasing. Further, the value of ε is above 200 for almost all samples, indicating that Ag substitution brings high anharmonicity to the structure since ε was usually in the range of 10-100 for simple semiconductor systems[23, 48]. This is reasonable because $AgInTe_2$ possesses much low melting point and high thermal expansion coefficient as compared with those in $CuInTe_2$[58]. Thus, the bonding strength between Ag and Te atoms is much lower than that between Cu and Te atoms, resulting in the prominent strain field fluctuation scattering to lattice phonons. When Ag content is about x = 0.2, i.e. at which pseudocubic structure is obtained for high power factor, the κ_L is 1.84 $Wm^{-1}K^{-1}$ at room temperature, only about half of that in $CuIn_{0.8}Ga_{0.2}Te_2$[59], while both materials possess almost the same atomic ratio and mass difference between the substituted and host atoms.

3.4 *ZT* value

Fig. 12(a) displays the temperature dependence of *ZT* values for $Cu_{1-x-\delta}Ag_xInTe_2$. Due to the band degeneration and strong strain-field fluctuation induced phonon scattering by Ag substitutions, the *ZT* values of $Cu_{1-x-\delta}Ag_xInTe_2$ are greatly improved. The *ZTs* in HP-$Cu_{0.75}Ag_{0.2}InTe_2$ and HP-$Cu_{0.88}Ag_{0.1}InTe_2$ achieve 1.24 and 1.10 at 850 K, respectively. The *ZT* values at 700 K *vs* η are plotted in Fig. 12(b). The literature data of chalcopyrite compounds are also presented. Among all of chalcopyrite compounds, $CuInTe_2$ is the one possesses η mostly close to unity in I-III-VI_2 chalcopyrites[21], thus the band splitting of $CuInTe_2$ is not as not large as the other compounds with serious lattice distortion. $Cu_{1-x}Ag_xInTe_2$ could be a typical chalcopyrite system, as the host compounds $CuInTe_2$ and $AgInTe_2$ possess appropriately high (>1) and low (<1) η values respectively and reasonable lattice mismatch, yielding an infinite solid solution. It is convincing that the power factor remains in the optimal level when η is around 1 in this solution system. By combining the dramatically reduction in thermal conductivity, high *ZT* values are achieved in this chalcopyrite system finally. All the high *ZT* values are located at around $\eta \approx 1$, in agreement with the "unity-η rule" for good chalcopyrite TE materials.

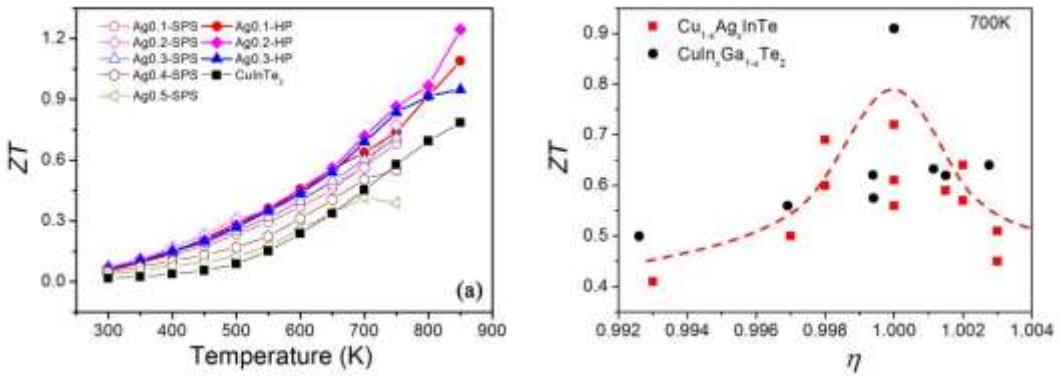

Fig. 12. (a) Dimensional thermoelectric figure of merit as a function of temperature for $Cu_{1-x-\delta}Ag_xInTe_2$($x$ = 0 - 0.5); (b) *ZT* value as a function of distortion parameter η at 700 K for $Cu_{1-x-\delta}Ag_xInTe_2$, $CuInTe_2$[14, 16], and $Cu(In_xGa_{1-x})Te_2$[15,18,59].

4. Summary

A series of polycrystalline $Cu_{1-x-\delta}Ag_xInTe_2$ samples has been successfully synthesized. The crystal structure and TE properties were investigated. The ideal

pseudocubic chalcopyrite structure without long range distortion is achieved at the composition with *x* around 0.2. Silver substitution essentially affects the valence band structure and the hole transport of $Cu_{1-x-\delta}Ag_xInTe_2$, leading to a decreased band gap and electrical conductivity. The optimal power factor was achieved when η is in the range of $1.00 < \eta < 1.02$, which confirms the "unity-η rule". As well, the lattice thermal conductivity is significantly depressed due to the extra point defect scattering to phonons in the solid solutions. Further analysis shows that the strain-field fluctuations play a dominated role in the κ_L reduction. A high *ZT* of 1.24 was obtained in the HP- $Cu_{0.75}Ag_{0.2}InTe_2$ sample. The hole mobility is obviously affected in the $Cu_{1-x-\delta}Ag_xInTe_2$ structure since the primary hole transport channels are mainly contributed from Cu-chalcogenide chemical bonds in diamond-like compounds[60, 61]. This tells us that the III-elements such as Ga or Al may be more effective to optimize thermoelectric properties because the mobility could be rarely affected[18,59]. Nevertheless, the pseudocubic structure is expected to be a powerful factor to achieve high electronic transport in these non-cubic diamond-like compounds.

Acknowledgements

This work was supported by National Basic Research Program of China (973-program) under Project No. 2013CB632501, National Natural Science Foundation of China (NSFC) under the Nos. 11234012 and 51302300, the Key Research Program of Chinese Academy of Sciences (Grant No. KGZD-EW-T06), and International S&T Cooperation Program of China (2015DFA51050). A part of the work was made within the MOU between SICCAS and MPI CPfS.

References:

1. Goldsmid HJ. *Thermoelectric Refrigeration*. New York: Plenum Press; 1964.
2. Nolas GS, J.Sharp, H.J.Goldsmid. *Thermoelectrics: Basic Principles and New Materials Developments*: Springer; 2001.
3. Pei YZ, Shi XY, LaLonde A, Wang H, Chen LD, Snyder GJ. Convergence of electronic bands for high performance bulk thermoelectrics. *Nature*. May 2011, 473(7345), 66-69.
4. Snyder GJ, Toberer ES. Complex thermoelectric materials. *Nature Materials*. Feb

2008,7(2), 105-114.

5. B. C. Sales , D. Mandrus , R. K. Williams , *Science*, 1996 , 272 , 1325 .
6. C. Uher , J. Yang , S. Hu , D. T. Morelli , G. P. Meisner , *Phys. Rev. B* 1999 , 59 , 8615 .
7. Liu W, Tan XJ, Yin K, et al. Convergence of Conduction Bands as a Means of Enhancing Thermoelectric Performance of n-Type $Mg_2Si_{1-x}Sn_x$ Solid Solutions. *Phys.Rev. Lett.*, 2012, 108(16).
8. H.Liu, X. Shi, F. Xu, L. Zhang,W. Zhang, L. Chen, Q. Li,C. Uher, T. Day and G. J. Snyder, Copper ion liquid-like thermoelectrics, *Nature materials*, 2012, 5 (11), 422-425
9. Shi X, Xi L, Fan J, Zhang W, Chen L. Cu-S Bond Network and Thermoelectric Compounds with Complex Diamondlike Structure. *Chem. Mater.*, 2011, 22(22), 6029-6031.
10. Cho JY, Shi X, Salvador JR, et al. Thermoelectric properties and investigations of low thermal conductivity in Ga-doped Cu_2GeSe_3. *Phys. Rev. B.*, 2011, 84(8), 085207.
11. Skoug EJ, Cain JD, Morelli DT. High thermoelectric figure of merit in the Cu_3SbSe_3-Cu_3SbS_4 solid solution. *Appl. Phys. Lett.*, 98(26), 261911-261913.
12. Skoug EJ, Morelli DT. Role of Lone-Pair Electrons in Producing Minimum Thermal Conductivity in Nitrogen-Group Chalcogenide Compounds. *Phys. Rev. Lett.*, 2011, 107(23), 235901.
13. Lu X, Morelli DT, Xia Y, et al. High Performance Thermoelectricity in Earth-Abundant Compounds Based on Natural Mineral Tetrahedrites. *Adv. Ener. Mater.*, Mar 2013, 3(3), 342-348.
14. Liu R, Xi L, Liu H, Shi X, Zhang W, Chen L. Ternary compound $CuInTe_2$: a promising thermoelectric material with diamond-like structure. *Chem. Comm.*, 2012, 48(32), 3818-3820.
15. Plirdpring T, Kurosaki K, Kosuga A, et al. Chalcopyrite CuGaTe2: A High-Efficiency Bulk Thermoelectric Material. *Adv. Mater.* , 2012, 24(27), 3622-3626.
16. Kosuga A, Plirdpring T, Higashine R, Matsuzawa M, Kurosaki K, Yamanaka S. High-temperature thermoelectric properties of $Cu_{1-x}InTe_2$ with a chalcopyrite structure. *Appl. Phys. Lett.*, 2012,100(4), 042108.
17. Shi XY, Huang FQ, Liu ML, Chen LD. Thermoelectric properties of tetrahedrally

bonded wide-gap stannite compounds $Cu_2ZnSn_{1-x}In_xSe_4$. *Appl. Phys. Lett.*, 2009,94(12),122103-122103.

18. Li Y, Meng Q, Deng Y, et al. High thermoelectric performance of solid solutions $CuGa_{1-x}In_xTe_2$ (x = 0–1.0). *Appl.Phys. Lett.*, 2012, 100(23), 231903 .
19. Aikebaier Y, Kurosaki K, Sugahara T, Ohishi Y, Muta H, Yamanaka S. High-temperature thermoelectric properties of non-stoichiometric $Ag_{1-x}InTe_2$ with chalcopyrite structure. *Mater. Sci.& Eng.,: B.* 2012, 177(12), 999-1002.
20. Yusufu A, Kurosaki K, Kosuga A, et al. Thermoelectric properties of $Ag_{1-x}GaTe_2$ with chalcopyrite structure. *Appl. Phys. Let.*, 99(6), 061902-061903.
21. Zhang J, Liu R, Cheng N, et al. High-Performance Pseudocubic Thermoelectric Materials from Non-cubic Chalcopyrite Compounds. *Adv. Mater.*, 2014, 26(23), 3848-3853.
22. Jiawei Zhang , Wenqing Zhang, Xun Shi, Bo B. Iversen, etal. Designing high-performance layered thermoelectric materials through orbital engineering, *Nature comm.*, 2016, 7, 10892
23. Yang J, Meisner GP, Chen L. Strain field fluctuation effects on lattice thermal conductivity of ZrNiSn-based thermoelectric compounds. *Appl. Phys. Lett.*, 2004, 85(7), 1140-1142.
24. Callaway J, von Baeyer HC. Effect of Point Imperfections on Lattice Thermal Conductivity. *Phys. Rev.*, 1960, 120(4), 1149.
25. Prabukanthan P, Dhanasekaran R. Growth of $CuInTe_2$ single crystals by iodine transport and their characterization. *Mater. Res. Bull.*, 2008;,43(8-9),1996-2004.
26. Moustafa AM, El-Sayad EA, Sakr GB. Crystal structure refinement of $Cu_xAg_{1-x}InTe_2$ bulk material determined from X-ray powder diffraction data using the Rietveld method. *Crys. Res.&.Tech.*, 2004;39(3), 266-273.
27. Fan J, Liu H, Shi X, Bai S, Shi X, Chen L. Investigation of thermoelectric properties of $Cu_2Ga_xSn_{1-x}Se_3$ diamond-like compounds by hot pressing and spark plasma sintering. *Acta Mater.*, 2013, 61(11), 4297-4304.
28. Akselrud L, Grin Y. WinCSD: software package for crystallographic calculations (Version 4). *J. Appl. Cryst.*,2014, (47), 803-805.

29. Marin G, Rincon C, Wasim SM, Power C, Perez GS. Temperature dependence of the fundamental absorption edge in $CuInTe_2$. *J. Appl. Phys.* , 1997, 81(11), 7580-7583.

30. El-Sayad EA, Sakr GB. Effect of composition on the optical properties of the quaternary $Cu_xAg_{1-x}InTe_2$ thin films. *Phys. Sta. Sol. (a).* 2003, 198(1), 188-196.

31. Jagomägi A, Krustok J, Raudoja J, et al. Photoluminescence and Raman spectroscopy of polycrystalline $AgInTe_2$. *Thin Solid Films.,* 2005, 481(0), 246-249.

32. El-Korashy A, Abdel-Rahim MA, El-Zahed H. Optical absorption studies on $AgInSe_2$ and $AgInTe_2$ thin films. *Thin Solid Films.,* 1999, 338(1–2), 207-212.

33. Zhang, Yubo, Xi, Lili, Wang, Youwei, Zhang, Jiawei, Zhang, Peihong, Zhang, Wenqing, Electronic properties of energy harvesting Cu-chalcogenides: p–d hybridization and d-electron localization, *Comp, Mater. Sci.,* 2015, 108, 239-249

34. Aikebaier Y, Ken K, Yuji O, Hiroaki M, Shinsuke Y. Thermoelectric Properties of Chalcopyrite-Type $CuGaTe_2$ with Ag Substituted into the Cu Sites. *J. J. Appl. Phys.*, 2013,52(8R), 081801.

35. Villarreal MA, Chalbaud LMd, Fernzndez BJ, A, Pirela M. Preparation and electrical characterization of the compound $CuAgGeSe_3$. *J. Phys. Conf. Seri.* 2009, 167(1), 012045.

36. Vining CB. A Model For The High-Temperature Transport-Properties Of Heavily Doped N-Type Silicon-Germanium Alloys. *J. Appl. Phys.* 1991,69(1),331-341.

37. Cheng N, Liu R, Bai S, Shi X, Chen L. Enhanced thermoelectric performance in Cd doped $CuInTe_2$ compounds. *J. Appl. Phys.*, 2014, 115(16), 163705.

38. Rowe JE, Shay JL. Extension of the Quasicubic Model to Ternary Chalcopyrite Crystals. *Phys. Rev. B,* 1971, 3(2), 451-453.

39. Artus L, Bertrand Y, Ance C. Crystal-field and spin-orbit interactions at the fundamental gap of $AgGaSe_2$ chalcopyrite compound. *J. Phys. C: Solid State Phys.*, 1986;19(29):5937.

40. Shay J, Wernick J. Ternary Chalcopyrite Crystals: Growth, Electronic Structure, and Applications. Pergamon, New York; 1975.

41. X. Shi, L. Chen & C. Uher, Recent advances in high-performance bulk thermoelectric materials, *Int. Mater. Rev.,* DOI 10.1080/0906608, 2016, 1183075

42. M. Beekman, M.Baitinger , H Borrmann, W. K. Schnelle, GS Nolas, Yu Grin, Preparation and Crystal Growth of $Na_{24}Si_{136}$, *J. Am. Chem. Soc.*, 2009, 131, 9642-9643

43. J. Schmidt, R. Niewa, M. Schmidt, et al., Spark plasma sintering effect on the decomposition of MgH_2, *J. Am. Ceram. Soc.*, 2005, 88, 1870-1874

44. Schmidt, J; Schnelle, W; Grin, Y; et al. Pulse plasma synthesis and chemical bonding in magnesium diboride, *Solid State Science*, 2003, 5(4), 535-539

45. Morelli DT, Jovovic V, Heremans JP. Intrinsically minimal thermal conductivity in cubic I-V-VI_2 semiconductors. *Phys. Rev. Lett.*, 2008,101(3), 035901.

46. Kurosaki K, Yamanaka S. Low-thermal-conductivity group 13 chalcogenides as high-efficiency thermoelectric materials. *Phys. Stat. soli., (a).* 2013;210(1):82-88.

47. Bodnar' IV. Optical and thermal properties of $CuAl_xIn_{1-x}Te_2$ solid solutions. *Semiconductors.* 2003/11/01 2003;37(11):1247-1251.

48. Liu M-L, Chen IW, Huang F-Q, Chen L-D. Improved Thermoelectric Properties of Cu-Doped Quaternary Chalcogenides of $Cu_2CdSnSe_4$. *Adv. Mater.*, 2009, 21(37), 3808-3812.

49. Abeles B. Lattice Thermal Conductivity of Disordered Semiconductor Alloys at High Temperatures. *Phys. Rev.*, 1963,131, 1906.

50. Meisner GP, Morelli DT, Hu S, Yang J, Uher C. Structure and lattice thermal conductivity of fractionally filled skutterudites: Solid solutions of fully filled and unfilled end members. *Phys. Rev. Lett.*, 1998, 80(16), 3551-3554.

51. Nolas GS, Cohn JL, Slack GA. Effect of partial void filling on the lattice thermal conductivity of skudderudites. *Phys. Rev. B.* 1998, 58(1), 164-170.

52. Gascoin F, Ottensmann S, Stark D, Haïle S, Snyder G. Zintl Phases as Thermoelectric Materials: Tuned Transport Properties of the Compounds $Ca_xYb_{1-x}Zn_2Sb_2$. *Adv. Funct. Mater.*, 2005, 15(11), 1860-1864.

53. Toberer ES, May AF, Melot BC, Flage-Larsen E, Snyder GJ. Electronic structure and transport in thermoelectric compounds AZn_2Sb_2 (A = Sr, Ca, Yb, Eu). *Dalton Trans.*,2010, 39(4),1046-1054.

54. Shi X, Yang J, Bai S, et al. On the Design of High-Efficiency Thermoelectric Clathrates

through a Systematic Cross-Substitution of Framework Elements. *Adv. Funct. Mater.*, 2009, 20(5), 755-763.

55. Jovovic V, Thiagarajan SJ, Heremans JP, Khokhlov D, Komissarova T, Nicorici A. High-temperature thermoelectric properties of $Pb_{1-x}Sn_xTe$: In. *Thermoelectric Power Generation.* 2008,1044,141-146480.
56. H. Julian G. Goldsmid: *Introduction To Thermoelectricity*. 2010.
57. Fernández B, Wasim SM. Sound Velocities and Elastic Moduli in $CuInTe_2$ and $CuInSe_2$. *Phys. Stat. soli. (a),* 1990, 122(1), 235-242.
58. Slack GA. Effect of Isotopes on Low-Temperature Thermal Conductivity. *Phys.Rev.*, 1957, 105(3), 829-831.
59. Y. Qin, X. Shi, L. Chen, et al, Optimized thermoelectric properties in pseudocubic diamond-like $CuGaTe_2$ compounds, *J. Mater. Chem. A*, 2016, 4, 1277.
60. Kumar V, Sastry BSR. Relationship between the thermal expansion coefficient, plasmon energy, and bond length of ternary chalcopyrite semiconductors. *J. Phys. & Chem. of Solid.,* 2002, 63(1), 107-112.
61. Xi L, Zhang YB, Shi XY, et al. Chemical bonding, conductive network, and thermoelectric performance of the ternary semiconductors $Cu_2Sn(Se, S)_3$ from first principles. *Phys. Rev. B.* 2012, 86(15), 155201.